Cherenkov second-harmonic Talbot effect in one-dimension nonlinear photonic crystal

Xiaohui Zhao,[1] Yuanlin Zheng,[1,2,3] Huaijin Ren,[1] Ning An,[1] and Xianfeng Chen[1,*]

[1]*State Key Laboratory of Advanced Optical Communication Systems and Networks, Department of Physics and Astronomy, Shanghai Jiao Tong University, 800 Dongchuan Road, Shanghai 200240, China*

[2]*Key Laboratory for Laser plasmas (Ministry of Education), Shanghai Jiao Tong University, 800 Dongchuan Road, Shanghai 200240, China*

[3]*e-mail: 5040729023@sjtu.edu.cn*

**Corresponding author: xfchen@sjtu.edu.cn*

Received July 25, 2014; revised September 15, 2014; accepted September 15, 2014; posted September 16, 2014 (Doc. ID 217798); published October 9, 2014

We demonstrate a new method to generate second-harmonic Talbot effect through degenerate Cherenkov radiation in one-dimension anomalous-dispersion-like nonlinear photonic crystals. In anomalous-dispersion-like medium, the degenerated nonlinear Cherenkov radiation can be achieved and is parallel to domain walls, of which the intensity is adjusted by the second-order nonlinear coefficient. In this system the one-dimension nonlinear photonic crystal can be regarded as a nonlinear grating, which is necessary for nonlinear Talbot effect. This is a new method to generate enhanced nonlinear Talbot effect in addition to the quasi-phase-matching technique reported previously.

OCIS codes: (190.0190) Nonlinear optics; (070.6760) Talbot and self-imaging effects; (190.2620) Harmonic generation and mixing.

http://dx.doi.org/10.1364/OL.39.005885

The Talbot effect [1] or the self-imaging effect is a Fresnel diffraction phenomenon in which a grating or other periodic structure replicates itself at regular distances away from the grating plane [2]. It holds a variety of applications in classical optics, such as imaging processing and synthesis, photolithography, optical testing and metrology, optical computing, spectrometry, microscopy [3,4], x-ray phase imaging [5], etc. Recently, the counterpart of Talbot effect in nonlinear optics or nonlinear Talbot effect was experimentally observed in 1D and 2D nonlinear photonic crystals [6]. The observed self-images are produced by collinear or quasi-phase-matching (QPM) second harmonic generation (SHG) [7]. It provides a new avenue to acquire images of second-order susceptibility-modulated structures and improves the imaging resolution. However, since QPM is a narrow-band harmonic technique, the wavelength of the input wave must be selected, which limits its application in nonlinear Talbot effect. On the other hand, as an automatic longitudinal phase-matching process, nonlinear Cherenkov radiation (NCR) [8] can provide more flexible matching wavelengths with corresponding phase-matching angles.

Cherenkov-type nonlinear process has been thoroughly discussed in second-order harmonic generation, high-order harmonic generation [9–11], sum frequency generation [12,13], and difference frequency generation [14]. The basic feature of NCR is that the phase velocity of the fundamental beam exceeds that of the harmonic radiation. This restricts such phenomenon in the regime of normal dispersion. Later, researchers demonstrated that the phase velocity of nonlinear polarization can be accelerated by domain walls (and also enhanced by them) [15–17], leading to the generation of NCR at anomalous dispersion condition [18].

In this Letter, we demonstrate, in both theory and experiment, the Cherenkov second-harmonic Talbot effect in MgO-doped periodically poled $LiNbO_3$ (PPLN) crystals. The intensity of degenerate NCR under anomalous dispersion that propagates along the domain walls is modulated by the second-order nonlinear coefficient. Here the PPLN sample is regarded as a second-order nonlinear grating about $\chi^{(2)}$, which is necessary to realize the nonlinear Talbot effect. As a longitudinal phase-matching process, the conversion efficiency of NCR is much higher than the phase-mismatching process. It can greatly enhance the intensity of the nonlinear Talbot self-images.

Under normal dispersion, the internal emission angle of NCR with respect to the domain wall $\theta = \arccos(n_1/n_2)$, where n_1 and n_2 denote the wave vectors of the fundamental wave (FW) and second harmonic (SH), respectively. When $n_1 > n_2$, it turns to be anomalous dispersion. The internal emission angle $\theta = \arccos((n_1/n_2)\cos\alpha)$, where α is the incident angle of FW in the crystal. Under the special situation: $\cos\alpha = n_2/n_1$, the emission angle of NCR is zero and the Cherenkov pair degenerates to a forward-propagating wave front. The phase-matching geometries are illustrated in Fig. 1. Besides NCR, nonlinear Raman-Nath diffraction (RND) can also be observed. The bright spots in Fig. 1(b) represent the phase matching nonlinear RND. The internal emission angle of mth order RND $\beta = \arcsin(mG/k_{2\omega})$, where $G = 2\pi/\Lambda$ is the reciprocal

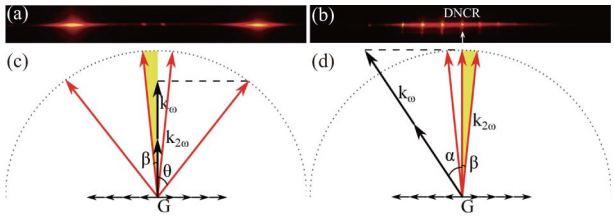

Fig. 1. Recorded patterns of the Raman-Nath diffraction and NCR under (a) normal dispersion and (b) anomalous dispersion, respectively. (c) and (d) are the phase-matching geometries.

vector of the domains structure, and Λ is the period of the domains structure, $k_{2\omega}$ is the wave vector of the SH wave.

In our experiment, we use a z-cut periodically poled 5 mol. % MgO:$LiNbO_3$ sample of the size 10 mm(x)× 5 mm(y) × 1 mm(z), which is fabricated through the electric-field poling technique at room temperature. The poling period $\Lambda = 13.86$ μm and the duty ratio is 1:1. The light source is an optical parametric amplifier (TOPAS, Coherent Inc.) generating 80 femtosecond pulses (1000 Hz rep. rate) at wavelengths tunable from 280 to 2600 nm. The laser beam is loosely focused into the sample by a 250-mm focal lens. The working temperature is 19°C. According to the Sellmeier equation [19], for pump light with wavelength longer than 1024 nm, the refractive index of ordinary-polarized FW is larger than that of extraordinary-polarized SH wave, which mimics anomalous dispersion [Fig. 2(a)].

At first, the sample is illuminated along y axis with the e-polarized laser beam with wavelength center at 1250 nm. The far-filed image on the screen is shown in Fig. 1(a), which comprises two RND spots close to the fundamental spot and a pair of NCR spots. The self-images of nonlinear Talbot effect can be only observed in the Fresnel diffraction zone, while Raman-Nath spots are the diffraction pattern presented in the far-field. When switching the laser beam to be o-polarized and the incident angle α satisfies the degenerate NCR situation, the far-field diffraction pattern [Fig. 1(b)] is much brighter than that in Fig. 1(a). It is easy to understand that NCR is an autokinetic phase-matching process that has higher conversion efficiency than the phase-mismatched collinear SHG. The spot in the middle is the degenerate NCR, and the three symmetrical dot pairs with different emission angles are first, second, and third RND from inner to outer.

In Fig. 2(b), we present the experimentally measured values of FW incident angles, which satisfied the

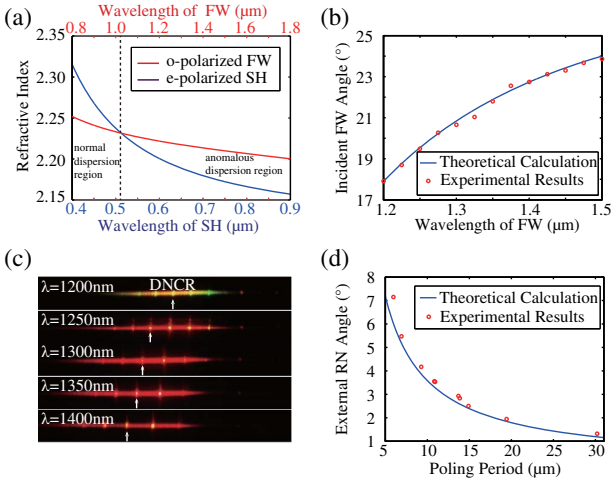

Fig. 2. (a) Theoretical refractive indices of ordinary-polarized fundamental beam and extraordinary-polarized second harmonic beam inside the crystal. (b) External FW incident angle for DNCR versus its wavelength. (c) Evolution of recorded patterns varying with the fundamental wavelength. (d) External RN angle β as a function of the poling period of the crystal. Theoretical prediction (solid curves) and experimental results (signs) are well in agreement with each other.

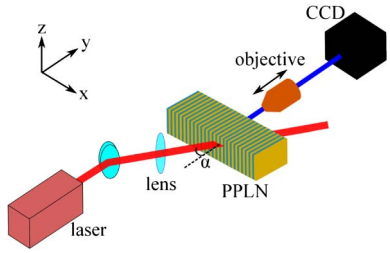

Fig. 3. Schematic setup.

condition of degenerated NCR, varying with its wavelength. The evolution of output pattern recorded on the screen is shown in Fig. 2(c). The dependence of external RND emission angle ($m = 1$) on domain period is verified experimentally by using ten samples with different poling periods (5.97, 6.92, 9.27, 10.83, 10.92, 13.7, 13.86, 14.9, 19.43, and 30.2 μm) [Fig. 2(d)].

To observe the degenerate Cherenkov Talbot effect, we use a 40× objective lens with N.A. = 0.65 (1.2 mm depth of focus and 4.65 mm working distance) moving along the y axis near the back of the sample, which was controlled by a precision translation stage (see Fig. 3). The generated SH is projected onto a CCD camera. The nonlinear coefficient used in our process is d_{13} as the fundamental beam is o-polarized and harmonic wave is e-polarized. In ferroelectric domain structure, d_{13} at the domain walls is different from that inside the domain [15–17]. So the intensity patterns of generated SH wave at the output surface have the same periodicity with domain structures of the sample.

Figure 4(a) illustrates the domain structure of PPLN. The SH pattern at the output face of the crystal is

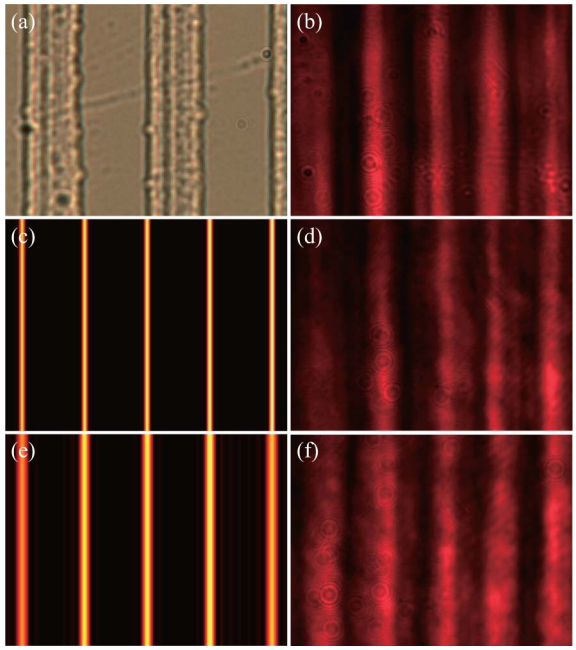

Fig. 4. Domain structure and NCR Talbot self-images. (a) The domain structure of the PPLN crystal recorded by an Olympus BX15 microscope in top view. (b) Intensity distribution at the output plan. The self-images at (c) first and (e) second Talbot plane have been simulated, and the experimental results are given as (d) and (f), respectively.

recorded in Fig. 4(b) with FW center at 1250 nm. The bright lines refer to the domain walls. We measured the separation distance of two streaks by moving the objective along the x axis. The result is 7 μm, which is approximately equal to the distance from a domain wall to the adjacent one, with the domain period of the sample of 13.86 μm. Therefore, the period of the nonlinear grating (i.e., PPLN) for self-imaging is $\Lambda/2$ and the Talbot length is obtained by $y_T = \Lambda^2/\lambda$, where λ is the wavelength of FW. The width of the domain walls is not as thin as expected, which can be ascribed to two aspects: one is the scattering of the defects at domain walls [20], and the other is the mixture of nondegenerate NCR in SH pattern as the pump bandwidth about 75 nm.

Figures 4(c) and 4(e) are the simulated SH patterns on the first ($y = y_T$) and second ($y = 2y_T$) Talbot planes, respectively. The width of the domain wall is set to be 0.5 μm, and $y_T = 154$ μm as the input beam is assumed a parallel beam with the size of 100 μm. Experimentally, first [Fig. 4(d)] and second [Fig. 4(f)] Talbot images were recorded at $y = 165$ μm and $y = 352$ μm. There is discrepancy between the Talbot length calculated in theory and measured in experiments. As the FW is a Gaussian beam, the wave profile should be taken into account, and the Talbot length should be modified by the square of the ratio of the beam radii at the observation and object plans. The bright region in second Talbot image is wider than that in first Talbot image, which is due to the confinement of beam size of input wave, consistent with the simulation.

In conclusion, the nonlinear Talbot effect enhanced by degenerate NCR can be generated in the anomalous-dispersion-like medium. We experimentally demonstrated degenerated Cherenkov SH patterns in the far-field and Fresnel diffraction zone. In the far-field, the phase-matching condition, angle-dependence of the fundamental beam, and diffraction pattern were studied. In the Fresnel diffraction zone, we propose a scheme for Talbot effect and experimentally observed the first and second self-images. As a longitudinal automatic phase matching, our scheme enhances the intensity of nonlinear Talbot self-images and provides a new way to check the effect of ferroelectric domains in nonlinear process.

This work was supported in part by the National Basic Research Program 973 of China under Grant No. 2011CB808101, the National Natural Science Foundation of China under Grant Nos. 61125503, 61235009, and 61205110, the Foundation for Development of Science and Technology of Shanghai under Grant No. 13JC1408300, and in part by the Innovative Foundation of Laser Fusion Research Center.

References

1. H. Talbot, Philos. Mag. **9**(56), 401 (1836).
2. L. Rayleigh, Philos. Mag. **11**(67), 196 (1881).
3. K. Patorski, Prog. Opt. **27**, 1 (1989).
4. J. Wen, Y. Zhang, and M. Xiao, Adv. Opt. Photon. **5**, 83 (2013).
5. F. Pfeiffer, M. Bech, O. Bunk, P. Kraft, E. Eikenberry, C. Brönnimann, C. Grünzweig, and C. David, Nat. Mater. **7**, 134 (2008).
6. Y. Zhang, J. Wen, S. N. Zhu, and M. Xiao, Phys. Rev. Lett. **104**, 183901 (2010).
7. D. Liu, D. Wei, Y. Zhang, J. Zou, X. P. Hu, S. N. Zhu, and M. Xiao, Opt. Express **21**, 13969 (2013).
8. Y. Zhang, Z. D. Gao, Z. Qi, S. N. Zhu, and N. B. Ming, Phys. Rev. Lett. **100**, 163904 (2008).
9. C. Chen, J. Lu, Y. Liu, X. Hu, L. Zhao, Y. Zhang, G. Zhao, Y. Yuan, and S. Zhu, Opt. Lett. **36**, 1227 (2011).
10. Y. Sheng, W. Wang, R. Shiloh, V. Roppo, Y. Kong, A. Arie, and W. Krolikowski, Appl. Phys. Lett. **98**, 241114 (2011).
11. N. An, H. Ren, Y. Zheng, X. Deng, and X. Chen, Appl. Phys. Lett. **100**, 221103 (2012).
12. S. M. Saltiel, D. N. Neshev, W. Krolikowski, N. Voloch-Bloch, A. Arie, O. Bang, and Y. S. Kivshar, Phys. Rev. Lett. **104**, 083902 (2010).
13. A. S. Aleksandrovsky, A. M. Vyunishev, A. I. Zaitsev, A. A. Ikonnikov, and G. I. Pospelov, Appl. Phys. Lett. **98**, 061104 (2011).
14. C. D. Chen, X. P. Hu, Y. L. Xu, P. Xu, G. Zhao, and S. N. Zhu, Appl. Phys. Lett. **101**, 071113 (2012).
15. A. Fragemann, V. Pasiskevicius, and F. Laurell, Appl. Phys. Lett. **85**, 375 (2004).
16. X. Deng, H. Ren, H. Lao, and X. Chen, J. Opt. Soc. Am. B **27**, 1475 (2010).
17. Y. Sheng, Q. Kong, V. Roppo, K. Kalinowski, Q. Wang, C. Cojocaru, and W. Krolikowski, J. Opt. Soc. Am. B **29**, 312 (2012).
18. H. Ren, X. Deng, Y. Zheng, N. An, and X. Chen, Phys. Rev. Lett. **108**, 223901 (2012).
19. O. Gayer, Z. Sacks, E. Galun, and A. Arie, Appl. Phys. B **91**, 343 (2008).
20. S. I. Bozhevolnyi, J. M. Hvam, K. Pedersen, F. Laurell, H. Karlsson, T. Skettrup, and M. Belmonte, Appl. Phys. Lett. **73**, 1814 (1998).